nuclear fusion

PAPER • OPEN ACCESS

Target electron removal in C^{5+} + H collision

To cite this article: Saed J. Al Atawneh and K. Tkési 2022 *Nucl. Fusion* **62** 026009

OPEN ACCESS
IOP Publishing | International Atomic Energy Agency Nuclear Fusion
Nucl. Fusion **62** (2022) 026009 (6pp) https://doi.org/10.1088/1741-4326/ac3ac5

Target electron removal in C^{5+} + H collision

Saed J. Al Atawneh[1,2] **and K. Tőkési**[1,*]

[1] Institute for Nuclear Research (ATOMKI), 4026 Debrecen Bem tér 18/c, Hungary
[2] Doctoral School of Physics, Faculty of Science and Technology, University of Debrecen, P.O.400, Debrecen, Hungary

E-mail: tokesi@atomki.hu

Received 7 June 2021, revised 19 October 2021
Accepted for publication 17 November 2021
Published 17 December 2021

Abstract

We present target ionization and charge exchange cross sections in a collision between C^{5+} ion and H atom. We treat the collision dynamics classically using a four-body classical trajectory Monte Carlo (CTMC) and a four-body quasi-classical Monte Carlo (QCTMC) model when the Heisenberg correction term is added to the standard CTMC model via model potential. The calculations were performed in the projectile energy range between 1.0 keV/amu and 10 MeV/amu. We found that the cross sections obtained by the QCTMC model are higher than that of the cross sections calculated by the standard CTMC model and these cross sections are closer to the previous experimental and theoretical data. Moreover, for the case of ionization, we show that the interaction between the projectile and the target electrons plays a dominant role in the enhancement of the cross sections at lower energies.

Keywords: ion–atom collision, ionization, electron capture, classical trajectory Monte Carlo method, Heisenberg correction

(Some figures may appear in colour only in the online journal)

1. Introduction

Carbon ions are one of the main impurities in present tokamak plasmas, where carbon composites are used in first wall tiles. The impurity particles originate especially from the limiter and the vacuum vessel wall called diverter [1–3]. Small amounts of carbon impurities will be present in the International Thermonuclear Experimental Reactor (ITER), and the future devices may include materials that will release C^{q+} ions [2, 3]. The processes leading to impurity release are complex and still poorly understood, as are the mechanisms of impurity transport.

Collisions between multiply charged ions and atomic hydrogen have received considerable interest [4–8]. The motivation for studying these types of collision systems is not only because of the general scientific interest but also has significant practical importance in fusion related research [9–12]. For instance, the collisions between multiple charged ions and atomic hydrogen are important in determining the radiation losses and neutral beam heating efficiencies in tokamak plasmas [13–15]. For the latter case, the presence of impurities in the plasma limits the effectiveness of such heating. In order to heat and refuel a fusion reactor plasma, the depth of penetration of fast hydrogen atoms into the plasma before they get ionized and held by the magnetic field is key significant [16]. The successful injection of a beam of fast hydrogen atoms into a fusion reactor for heating purposes and refueling the plasma is contingent on the ability of the beam to penetrate the plasma, among other factors [16]. It is important to ensure that the rate of ionization is not too high to prohibit sufficient beam penetration, nor too low to allow a significant portion of the beam to pass straight through the plasma [16]. Therefore, the common plasma impurities like carbon, nitrogen, and oxygen are of special interest as well as metallic species sputtered from the container walls [17–19]. So, the accurate knowledge of various cross sections when the multiply charged ions of these elements colliding with hydrogen atoms are key important.

In this work, we will focus on the carbon ion and present the ionization (see equation (1)) and single capture (see equation (2)) cross sections to the projectile bound state in a

* Author to whom any correspondence should be addressed.

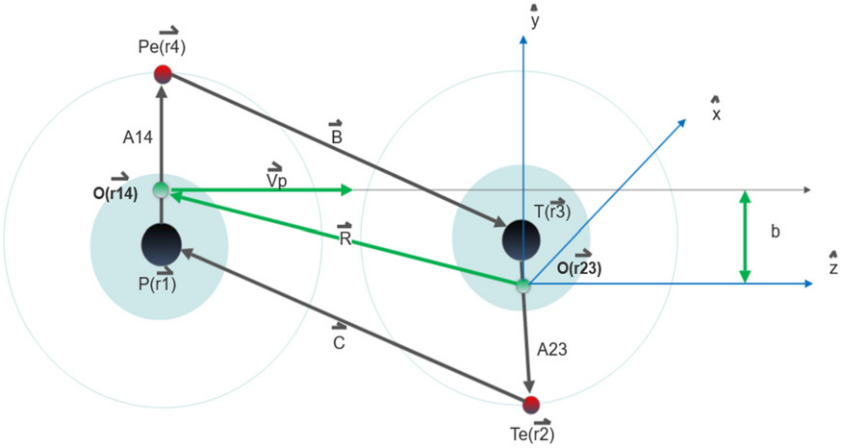

Figure 1. Schematic diagram for the four-body collisions. $\vec{A}_{14} = \vec{r}_4 - \vec{r}_1$, $\vec{B} = \vec{r}_4 - \vec{r}_3$, $\vec{A}_{23} = \vec{r}_3 - \vec{r}_2$, and $\vec{C} = \vec{r}_2 - \vec{r}_1$, in such way that $\vec{A}_{14} + \vec{A}_{23} + \vec{B} + \vec{C} = 0$. Also, $O(\vec{r}_{23})$ and $O(\vec{r}_{14})$ are the position vector of the center-of-mass of the target and projectile systems, respectively. b is the impact parameter.

collision between C^{5+} ion and H atom.

$$C^{5+} + H(1s) \rightarrow C^{5+} + H^{+} + e^{-}, \tag{1}$$

$$C^{5+} + H(1s) \rightarrow C^{4+} + H^{+}. \tag{2}$$

The collision dynamics are modeled classically utilizing a four-body classical trajectory Monte Carlo (CTMC) [20] and a four-body quasi-classical Monte Carlo (QCTMC) model [21, 22] when the Heisenberg potential is included to the standard CTMC model via model potential. Classically, when more than one electron is taken into account in the simulation, a necessary condition for stability of atomic or ionic formation is partly that the electrons are not allowed to collapse to the nucleus, and partly that the autoionization must be avoided. The effective factor enforcing this condition is introduced by the Heisenberg uncertainty principle $r_i p_i \geqslant \xi_H \hbar$, where r_i, p_i, and ξ_H are relative distance, the relative momentum of an electron to the ionic core (nucleus), and a dimensionless constant, respectively. For hydrogen atom, this condition is equivalent to the de Broglie–Bohr description of the hydrogen atom, the electron treated as a particle on an ellipse with wave-like properties. This leads naturally to the quantization of electron momentum and kinetic energy, and consequently a manifold of allowed energy states for the electron relative to the nucleus [23, 24]. Generalizing the calculation scheme of the QCTMC model, we apply it for our collisions system. Our calculations are in the range between 1.0 keV/amu and 10 MeV/amu. This energy range covers the typical energies of many astrophysical and laboratory plasmas, including the radiation losses and neutral beam heating efficiencies in tokamak plasmas. Atomic units are used throughout unless stated otherwise.

2. Theory

2.1. The four-body CTMC model

In this work, the four particles (target nucleus, target's electron, projectile's electron, and projectile nucleus) are described by their masses and charges. P stands for projectile nucleus, P_e for projectile electron, T for target nucleus, and T_e for target electron [25]. Our four-body calculation explicitly includes the electron–electron interaction. At the time ($t = -\infty$), we treat the four particles as two isolated particles, consisting of the C^{5+} projectile system (P, P_e) labelled as particles (1, 4), and the H target system (T, T_e) labelled as particles (2, 3) [25]. Initially, both the projectile (P, P_e) and the target (T, T_e) are in the ground state ($n, l = 1, 0$). The interactions among the particles are Coulombic ones [20, 25, 26]. Figure 1 shows the relative position vectors of our four-body collision system.

A micro-canonical ensemble characterizes the initial state of the target and projectile constrained to an initial binding energy of the given shell can be expressed as:

$$\rho_{E_0}(\vec{X}, \dot{\vec{X}}) = K_1 \delta(E_0 - E) = \delta\left(E_0 - \frac{1}{2}\mu_{a,b}\dot{\vec{X}}^2 - V(X)\right), \tag{3}$$

where K_1 is a normalization constant, E_0 is the ionization energy of the active electron, $V(X)$ is the electron and ionic-core potential, X is the length of the vector $\vec{X}$, and $\mu_{a,b}$ is the reduced mass of particles a and b. For the target system: $\vec{X} = \vec{A}_{23}$, $a = T$, $b = T_e$, and for the projectile system: $\vec{X} = \vec{A}_{14}$, $a = P$, $b = P_e$. According to the equation (3), the electronic coordinate is confined to the intervals where the equation (4) is verified:

$$\frac{1}{2}\mu_{a,b}\dot{\vec{X}} = E_0 - V(X) > 0. \tag{4}$$

The Hamiltonian of the system can be expressed as:

$$H = \sum_{i=1}^{n} p_i \dot{q}_i - L(q_i, \dot{q}_i, t), \tag{5}$$

where (q_i, p_i) are the position and momentums of the system, respectively. From equation (5), the Hamilton's equations are determined by

$$\dot{q}_i = \frac{\partial H}{\partial p_i}, \tag{6}$$

$$\dot{p}_i = -\frac{\partial H}{\partial q_i}, \tag{7}$$

where $i = p, t, e_p, e_t$. The Runge–Kutta–Gill method is employed to numerically integrate the equations of motions with an ensemble of about 1×10^6 primary trajectories for each energy [25]. To maintain statistical uncertainty less than 2%, a large number of trajectories are usually required. The total cross sections can by calculated by

$$\sigma_p = \frac{2\pi b_{\max}}{N} \sum_j b_j^{(P)}, \tag{8}$$

where $b_j^{(P)}$ is a given impact parameter that meets the conditions for process P with N being the total number of trajectories calculated, and $b_{\max}$ is a greatest value of the impact parameter that the above processes can occur [25]. The statistical uncertainty of the cross section is given by

$$\Delta\sigma = \sigma_p \left[\frac{N - N_P}{N N_P}\right]^{1/2}, \tag{9}$$

where N_P is the number of trajectories that satisfy the criteria for the process P.

2.2. The four-body QCTMC model

The QCTMC model is a one-step forward in the extension of the standard CTMC model improved by including quantum mechanical principles [21]. Generally, in the modified Hamiltonian effective potentials (V_H, which mimics the Heisenberg principle, and V_P, which mimics the Pauli principle) are typically added to the pure Coulomb inter-particle potentials [25]. Thus

$$H_{\mathrm{QCTMC}} = H_0 + V_H + V_P, \tag{10}$$

where H_0 is the standard Hamiltonian containing the total kinetic energy of all bodies as well as Coulomb potential terms for all particles. The correction terms are

$$V_H = \sum_{i=1}^{N} \frac{1}{m r_i^2} f\left(r_i, p_i; \xi_H; \alpha_H\right), \tag{11}$$

and

$$V_p = \sum_{i=1}^{N} \sum_{j=i+1}^{N} \frac{2}{m r_{ij}^2} f\left(r_{ij}, p_{ij}; \xi_p; \alpha_p\right) \delta_{s_i,s_j}, \tag{12}$$

where the i, j index the electrons. Also, $r_{ij} = r_j - r_i$ and relative momenta are:

$$P_{ij} = \frac{m_i p_j - m_j p_i}{m_i + m_j} \tag{13}$$

$\delta_{s_i,s_j} = 1$, if the ith and jth electrons have the same spin and 0 if they are different. Ultimately, the constraining potentials are chosen as

$$f\left(r_{\lambda\nu}, p_{\lambda\nu}; \xi, \alpha\right) = \frac{\xi^2}{4\alpha r_{\lambda\nu}^2 \mu_{\lambda\nu}} \exp\left\{\alpha\left[1 - \left(\frac{r_{\lambda\nu} p_{\lambda\nu}}{\xi}\right)^4\right]\right\}. \tag{14}$$

The hydrogen atom consists of one electron and one proton. As a consequence, the Heisenberg constrain was applied with the scale parameters, hardness ($\boldsymbol{\alpha_H} = 2.8$) and dimensionless constant ($\boldsymbol{\xi_H} = 0.9211$). The Heisenberg potential of the target is given by equation (15):

$$f\left(\vec{r}_{T,T_e}, \vec{P}_{T,T_e}; \varepsilon_H, \alpha_H\right) = \frac{{\xi_H}^2}{4\alpha_H \vec{r}_{T,T_e}^2 \mu_{T,T_e}} \exp\left\{\alpha_H\left[1 - \left(\frac{\vec{r}_{T,T_e}\vec{P}_{T,T_e}}{\xi_H}\right)^4\right]\right\}. \tag{15}$$

The Heisenberg correction should be considered also between an electron and ionic core of the projectile as follows:

$$f\left(\vec{r}_{P,P_e}, \vec{P}_{P,P_e}; \varepsilon_H, \alpha_H\right) = \frac{{\xi_H}^2}{4\alpha_H \vec{r}_{P,P_e}^2 \mu_{P,P_e}} \exp\left\{\alpha_H\left[1 - \left(\frac{\vec{r}_{P,P_e}\vec{P}_{P,P_e}}{\xi_H}\right)^4\right]\right\}. \tag{16}$$

Finally the Pauli correction term was included according to equation (17), as:

$$f\left(r_{ij}, p_{ij}; \xi_p; \alpha_p\right) = \frac{{\xi_p}^2}{4\alpha_p \vec{r}_{ij}^2 \mu_{ij}} \exp\left\{\alpha_P\left[1 - \left(\frac{\vec{r}_{ij}\vec{P}_{ij}}{\xi_p}\right)^4\right]\right\}. \tag{17}$$

According to figure 1, the equations of motion taking into account the Hamiltonian mechanics besides the correction terms to calculate the cross sections are as follows:

$$\begin{aligned}
\dot{\vec{P}}_p &= -\frac{\delta H_{\mathrm{QCTMC}}}{\delta \vec{r}_P} \\
&= \left[\frac{Z_P Z_{P_e}}{\left|\vec{r}_p - \vec{r}_{P_e}\right|^3}\left(\vec{r}_P - \vec{r}_{P_e}\right)\right. \\
&\quad - \left(-\frac{{\xi_H}^2}{2\alpha_H \vec{r}_{P,P_e}^4 \mu_{P,P_e}} - \frac{\left(\vec{P}_{P,P_e}\right)^4}{\mu_{P,P_e}{\xi_H}^2}\right) \\
&\quad \left.\times \exp\left\{\alpha_H\left[1 - \left(\frac{r_{P,P_e}P_{P,P_e}}{\xi_H}\right)^4\right]\right\}\right] \\
&\quad + \frac{Z_P Z_T}{\left|\vec{r}_P - \vec{r}_T\right|^3}\left(\vec{r}_P - \vec{r}_T\right) + \frac{Z_P Z_{T_e}}{\left|\vec{r}_P - \vec{r}_{T_e}\right|^3}\left(\vec{r}_P - \vec{r}_{T_e}\right),
\end{aligned} \tag{18}$$

$$\begin{aligned}
\dot{\vec{P}}_{P_e} &= -\frac{\delta H_{\mathrm{QCTMC}}}{\delta \vec{r}_{P_e}} \\
&= -\left[\frac{Z_P Z_{P_e}}{\left|\vec{r}_P - \vec{r}_{P_e}\right|^3}\left(\vec{r}_P - \vec{r}_{P_e}\right)\right.
\end{aligned}$$

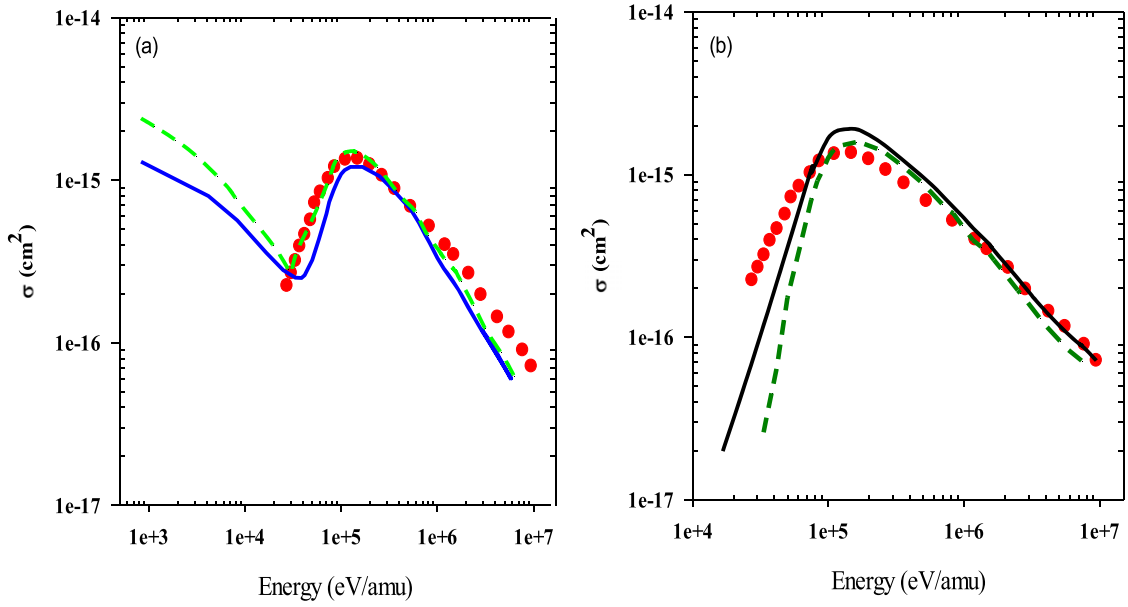

Figure 2. Target ionization cross sections in a collision between C^{5+} ion and H(1s) atom as a function of impact energy. (*a*) Blue solid line: the present four-body CTMC results. Green dashed line: the present four-body QCTMC results. Red circles: the three-body CTMC calculation by Janev and McDowell reference [26]; (*b*) dark green dashed line: the present reduced four-body CTMC, i.e. $V(2,4)=0$. Black solid line: the present reduced four-body QCTMC, i.e. $V(2,4)=0$. Red circles: the three-body CTMC calculation by Janev and McDowell reference [26].

$$
\begin{aligned}
&+\left(-\frac{{\xi_H}^2}{2\alpha_H \vec{r}^{\,4}_{P,P_e}\mu_{P,P_e}}-\frac{\left(\vec{P}_{P,P_e}\right)^4}{\mu_{P,P_e}{\xi_H}^2}\right)\\
&\times\exp\left\{\alpha_H\left[1-\left(\frac{r_{P,P_e}P_{P,P_e}}{\xi_H}\right)^4\right]\right\}\Bigg]\\
&-\frac{Z_T Z_{P_e}}{\left|\vec{r}_T-\vec{r}_{P_e}\right|^3}\left(\vec{r}_T-\vec{r}_{P_e}\right)-\left[\frac{Z_{T_e}Z_{P_e}}{\left|\vec{r}_{T_e}-\vec{r}_{P_e}\right|^3}\left(\vec{r}_{T_e}-\vec{r}_{P_e}\right)\right.\\
&-\left(-\frac{{\xi_P}^2}{2\alpha_P \vec{r}^{\,4}_{T_e,P_e}\mu_{T_e,P_e}}-\frac{\left(\vec{P}_{T_e,P_e}\right)^4}{\mu_{T_e,P_e}{\xi_H}^2}\right)\\
&\times\exp\left\{\alpha_p\left[1-\left(\frac{r_{T_e,P_e}P_{T_e,P_e}}{\xi_P}\right)^4\right]\right\}\Bigg],
\end{aligned}
\tag{19}
$$

$$
\begin{aligned}
\dot{\vec{P}}_T &= -\frac{\delta H_{\mathrm{QCTMC}}}{\delta \vec{r}_T}\\
&= -\frac{Z_P Z_T}{\left|\vec{r}_P-\vec{r}_T\right|^3}\left(\vec{r}_P-\vec{r}_T\right)-\left[\frac{Z_{T_e}Z_T}{\left|T_e-\vec{r}_T\right|^3}\left(\vec{r}_{T_e}-\vec{r}_T\right)\right.\\
&\quad+\left(-\frac{{\xi_H}^2}{2\alpha_H \vec{r}^{\,4}_{T,T_e}\mu_{T,T_e}}-\frac{\vec{P}_{T,T_e}{}^4}{\mu_{T,T_e}{\xi_H}^2}\right)\\
&\quad\times\exp\left\{\alpha_H\left[1-\left(\frac{r_{T,T_e}P_{T,T_e}}{\xi_H}\right)^4\right]\right\}\Bigg]\\
&\quad+\frac{Z_T Z_{P_e}}{\left|\vec{r}_T-\vec{r}_{P_e}\right|^3}\left(\vec{r}_T-\vec{r}_{P_e}\right),
\end{aligned}
\tag{20}
$$

$$
\begin{aligned}
\dot{\vec{P}}_{T_e} &= -\frac{\delta H_{\mathrm{QCTMC}}}{\delta \vec{r}_{T_e}}\\
&= -\frac{Z_P Z_{T_e}}{\left|\vec{r}_P-\vec{r}_{T_e}\right|^3}\left(\vec{r}_P-\vec{r}_{T_e}\right)-\left[\frac{Z_{T_e}Z_T}{\left|T_e-\vec{r}_T\right|^3}\left(\vec{r}_{T_e}-\vec{r}_T\right)\right.\\
&\quad+\left(-\frac{{\xi_H}^2}{2\alpha_H \vec{r}^{\,4}_{T,T_e}\mu_{T,T_e}}-\frac{\vec{P}_{T,T_e}{}^4}{\mu_{T,T_e}{\xi_H}^2}\right)\\
&\quad\times\exp\left\{\alpha_H\left[1-\left(\frac{r_{T,T_e}P_{T,T_e}}{\xi_H}\right)^4\right]\right\}\Bigg]\\
&\quad-\left[\frac{Z_{T_e}Z_{P_e}}{\left|\vec{r}_{T_e}-\vec{r}_{P_e}\right|^3}\left(\vec{r}_{T_e}-\vec{r}_{P_e}\right)\right.\\
&\quad-\left(-\frac{{\xi_P}^2}{2\alpha_P \vec{r}^{\,4}_{T_e,P_e}\mu_{T_e,P_e}}-\frac{\left(\vec{P}_{T_e,P_e}\right)^4}{\mu_{T_e,P_e}{\xi_H}^2}\right)\\
&\quad\times\exp\left\{\alpha_p\left[1-\left(\frac{r_{T_e,P_e}P_{T_e,P_e}}{\xi_P}\right)^4\right]\right\}\Bigg].
\end{aligned}
\tag{21}
$$

3. Result and discussion

3.1. Ionization

At first, let us begin with the target ionization channel when the target lost its electron and the projectile remains in the same charge state after the collisions.

Figure 2 shows our present ionization cross sections of the target as a function of impact energy. Our results are compared with the previous target ionization cross sections by

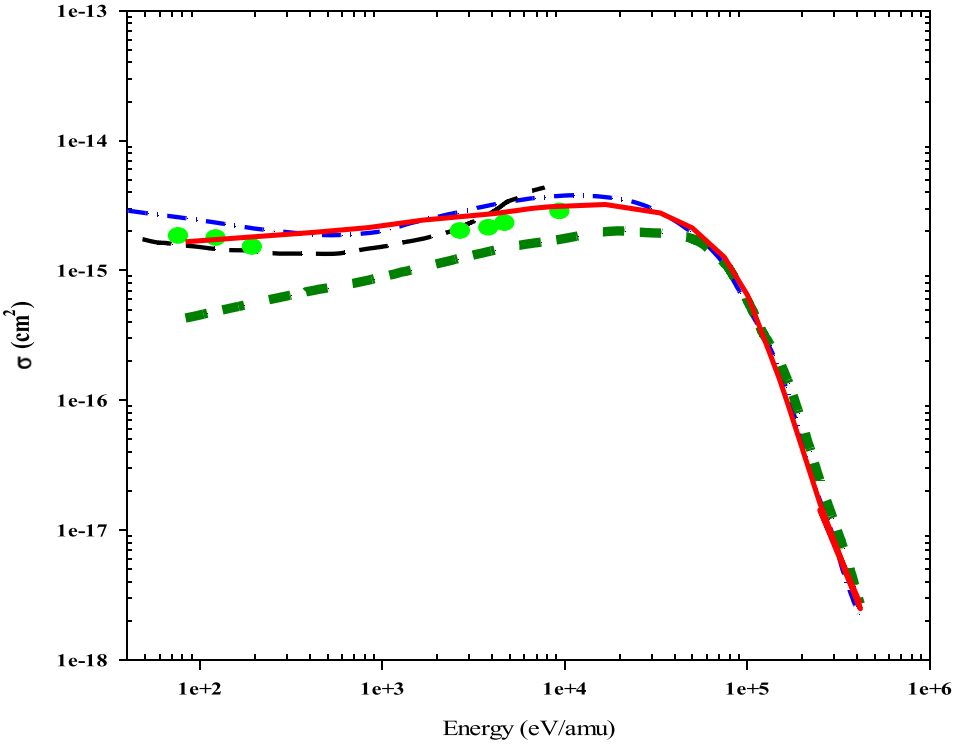

Figure 3. Electron capture cross sections of the projectile as a function of impact energy in a collision between C^{5+} ion with H atom. (*a*) Dark green dots: presents four-body CTMC results. Red solid line: presents four-body QCTMC results. Blue dashed-dots line: the three-body CTMC calculation by Janev and McDowell reference [26]. Black dashed line: the PSS method by Shipsey *et al* reference [9]. Green dashed line: experimental data by Crandall *et al* reference [34].

Janev [26]. It can be seen that the present standard four-body CTMC results are close to the previous classical simulation of Janev particularly between 0.1 MeV/amu and 1.0 MeV/amu impact energy. However, at lower than 40 keV/amu impact energies enhancements of the cross sections are obtained both for our standard four-body CTMC and four-body QCTMC approaches (see figure 2(*a*)). On the other hand, the four-body QCTMC cross sections are slightly higher than that of the results by the standard CTMC method and closer to the previous cross sections. The ionization of the target is limited to the time when the projectile (C^{5+}) overlap with hydrogen atom during the collisions. For understanding of the enhanced cross sections at lower energies, we can take into account the followings: (1) since the collision is much slower, the interaction time in the overlapping region is larger. (2) The slow collision may also indicate that the neutral target atom at least can treat as an enhanced electric dipole during the collision and the ionization probability can increase. (3) The repulsive electron–electron interaction dominant at low energy. In principle we performed a so called reduced four-body CTMC and QCTMC calculations when the electron–electron interaction was switched off ($V(2, 4) = 0$). To test our assumptions. The results were in agreement with our expectations. For the case of the reduced calculations the enhancement in the cross sections disappeared, emphases the importance of electron–electron repulsion. In addition, the reduced four-body CTMC approach shows an excellent agreement above 0.9 MeV/amu with the three-body calculations. Meanwhile, the reduced QCTMC shows quite differences in the energy range of 15 keV/amu to 0.9 MeV/amu (see figure 2(*b*)).

3.2. Electron capture

Electron capture by multiply charged ions play a key role to specify the penetration of the injection-heating [32]. It has also importance in the neutral beams diagnostic [33], and in astrophysics as an important mechanism that reduces the ionization [27–31, 34]. Therefore the accurate knowledge of the electron capture cross sections by multiply charged ions is crucial point in many cases like in understanding the atomic transport and spectral emissions spectroscopy.

Figure 3 shows our present cross sections σ_c (C^{4+}) for electron capture process of C^{5+} + H(1s) collision. Figure 3 also shows the previous results of the electron capture cross section by Janev and McDowell [26], Shipsey *et al* [9], and experimental data of Crandall *et al* [34]. Janev *et al* applied the three-body CTMC method to simulate a four body collision system of the C^{5+}+ H(1s), Shipsey *et al* used the perturbed stationary-state (PSS) method at low impact energy. The present four-body CTMC provide a good agreement with the theoretical data at higher impact energies. On the other hand, at low energies, the present four-body CTMC calculations underestimate the experimental and other theoretical observations (see figure 3). Similarly, to the case of ionization, however, a four-body QCTMC model provide a much higher cross sections and show an excellent agreement with previous results.

4. Conclusion

Target electron removal in C^{5+} + H collision were presented in the projectile energy range between 1.0 keV/amu and 10 MeV/amu and compared them with previously obtained theoretical and experimental results. A four-body CTMC and a four-body QCTMC model of the Kirschbaum and Wilets were used to calculate the ionization and charge exchange cross sections. According to our knowledge, this is the first time to present cross section data using the QCTMC method for this collision system. We found that the QCTMC method improved the cross section data significantly compared with the results of the standard CTMC method. We found also a reasonably good agreement between the experimental data and our results obtained by QCTMC method.

Acknowledgments

This work has been carried out within the framework of the EUROfusion Consortium and has received funding from the Euratom research and training programme 2014–2018 and 2019–2020 under Grant Agreement No. 633053. The views and opinions expressed herein do not necessarily reflect those of the European Commission.

ORCID iDs

Saed J. Al Atawneh https://orcid.org/0000-0003-1680-9667
K. Tőkési https://orcid.org/0000-0001-8772-8472

References

[1] Lawson K.D., Coffey I.H., Aggarwal K.M. and Keenan F.P. (JET-EFDA Contributors) 2013 *J. Phys. B: At. Mol. Opt. Phys.* **46** 035701
[2] Federici G. 2006 *Phys. Scr.* **T124** 1–8
[3] Lipschultz B. *et al* 2007 *Nucl. Fusion* **47** 1189–205
[4] Bendahman M., Bliman S., Dousson S., Hitz D., Gayet R., Hanssen J., Harel C. and Salin A. 1985 *J. Physique* **46** 561–72
[5] Toshima N. 1994 *Phys. Rev.* A **50** 3940–7
[6] Janev R.K., Ivanovski G. and Solov'ev E.A. 1994 *Phys. Rev.* A **49** R645–8
[7] Gallagher J.W., Bransden B.H. and Janev R.K. 1983 *J. Phys. Chem. Ref. Data* **12** 873–90
[8] Loarte A. *et al* 2007 Progress in the ITER Physics Basis Chapter 4: Power and particle control *Nucl. Fusion* **47** S203
[9] Shipsey E.J., Browne J.C. and Olson R.E. 1981 *J. Phys. B: At. Mol. Phys.* **14** 869–80
[10] McCullough R.W. 2001 *Phys. Scr.* **T92** 76–9
[11] Wilkie F.G. 1985 State-elective electron capture by multiply charged ions in atomic hydrogen *U-Thesis* Queen's University, Belfast (United Kingdom)
[12] Tillack M.S. *et al* 2013 *Nucl. Fusion* **53** 027003
[13] Barnett C.F. 1975 Atomic physics in the controlled thermonuclear research program *Report No. CONF-750705-4* United States
[14] Gusev V.K. *et al* 2011 *Nucl. Fusion* **51** 103019
[15] Ushigusa K. *et al* 1989 *Nucl. Fusion* **29** 265–76
[16] Riviere A.C. 2011 *Nucl. Fusion* **11** 363
[17] LaBombard B. *et al* 2017 *Nucl. Fusion* **57** 076021
[18] Wang F. *et al* 2018 *Plasma Phys. Control. Fusion* **60** 125005
[19] Olson R.E. and Salop A. 1977 *Phys. Rev.* A **16** 531–41
[20] Atawneh S.J.A., Asztalos Ö., Szondy B., Pokol G.I. and Tőkési K. 2020 *Atoms* **8** 31
[21] Kirschbaum C.L. and Wilets L. 1980 *Phys. Rev.* A **21** 834–41
[22] Wilets L. and Cohen J.S. 1998 *Contemp. Phys.* **39** 163–75
[23] Broglie L.D. 2006 *Phil. Mag. Lett.* **86** 411–23
[24] Thomas A. 2016 *J. Appl. Math.Theor. Phys.* **2** 1–15
[25] Al Alatwneh S.J. and Tokesi K. 2021 *J. Phys. B: At. Mol. Opt. Phys.* **54** 065202
[26] Janev R.K. and McDowell M.R.C. 1984 *Phys. Lett.* A **102** 405–8
[27] McCray R., Wright C. and Hatchett S. 1977 *Astrophys. J.* **211** L29
[28] Dalgarno A. and Butler S.E. 1978 *Com. Atom. Mol. Phys.* **7** 129–35
[29] Steigman G. 1975 *Astrophys. J.* **199** 642–6
[30] Christensen R.B., Watson W.D. and Blint R.J. 1977 *Astrophys. J.* **213** 712–5
[31] Butler S.E., Guberman S.L. and Dalgarno A. 1977 *Phys. Rev.* A **16** 500–7
[32] Hogan J.T. and Howe H.C. 1976 *J. Nucl. Mater.* **63** 151–7
[33] Equipe TFR 1978 Tokamak plasma diagnostics *Nucl. Fusion* **18** 647–731
[34] Crandall D.H., Phaneuf R.A. and Meyer F.W. 1979 *Phys. Rev.* A **19** 504–14